Title

Downslope Winds and Dust Storms in the Salton Basin Downslope Winds and Dust Storms in the Salton Basin

Journal

Monthly Weather Review, 147(7)

ISSN

0027-0644

Author

Evan, Amato T

Publication Date

2019-07-01

DOI

10.1175/mwr-d-18-0357.1

Peer reviewed

Downslope Winds and Dust Storms in the Salton Basin

AMATO T. EVAN*

Scripps Institution of Oceanography, University of California, San Diego La Jolla, California

ABSTRACT

The Salton Basin is a closed, sub-sea level basin located in extreme southeastern California. At the center of the basin lies the Salton Sea, the state's largest inland lake, which is surrounded by a desert landscape characterized by paleo lakebed surfaces, dry washes, alluvial fans and interdunes. Dust storms are common occurrence in this region. However, despite the regularity of dust outbreaks here, little is known about the meteorological processes responsible for these storms. Here I use observations and output from reanalysis to elucidate the meteorological controls on dust emission events in the Salton Basin during 2015–2018. Analysis of surface and upper air observations, satellite data, and reanalysis, suggest that the largest dust storms in the region are associated with an upper-level low centered near the coastline of western Canada, which directs a zonal low-level jet over the region. Flow blocking by a coastal mountain range results in isentropic drawdown of air in the lee of these mountains. Once surface warming at the floor of the Salton Basin is sufficient such that the density of the descending air is greater than that of the ambient air at the surface, the downslope windstorm reaches the desert floor and initiates dust emission. This process may also be accompanied by a downwind propagating hydraulic jump. These processes appear to be similar to those responsible for the strongest dust events in the Owens Valley, and may represent the main mechanisms for emission from other closed basins.

1. Introduction

The Salton Basin is a large (approximately 7000 km^2) closed, sub-sea level basin within the Sonoran Desert. The basin is hyper-arid, receiving on-average less than 100 mm of precipitation each year (Stephen and Gorsline 1975). Rainfall can occur in the winter months in association with the passage of extratropical cyclones or in the summer months due to monsoonal intrusions, where the latter predominately impacts the southernmost region of the Basin (Ives 1949). Although rare, it is possible for eastern North Pacific hurricanes to track through, as was the case for Hurricane Kathleen in 1976 (Gunther 1977). Daily average temperatures in the Basin during the winter months are 12-15^{o}C, and in the summer months are greater than 32^{o}C (Ives 1949), with summertime high temperatures in the Salton regularly above 40^{o}C (Stephen and Gorsline 1975; King et al. 2011).

The Salton Sea occupies the deepest point of the Salton Basin. Agricultural lands are found to the north and south of the Sea, and the Anza Desert lies to the immediately to its west (Fig 1a). The Basin is bounded to the west by the coastal Peninsular Mountain Ranges, and to the north and east by the southern section of the Transverse Mountain Ranges, which is comprised of the nearly 3,000 m high San Bernardino Mountains to the north, and the smaller (approximately 1,000 m in height) Orocopia Mountains to the east (Figs 1ab). The northern end of the Valley contains the Coachella Valley, and the city of Palm Springs, which gives way to the 800 m high Banning Pass (Figs 1ab). To the south the Salton Basin widens and is referred to as the Imperial Valley. Beyond the Imperial Valley, the surface elevations continue to rise until reaching the Colorado River Delta and then the Gulf of California. The morphology of the region surrounding the sea includes alluvial fans, sand and sand dunes, dry washes, paleo lakebed, and rock and vegetated surfaces (District 2016).

Throughout time the Salton Basin has periodically flooded as the Colorado River meandered and breached the basin, only to later dry when the Colorado's flow took a more southeastward route to the Gulf of California (Babcock 1974). In 1905, the Colorado River burst through a canal system designed to divert part of the river's flow into the Imperial Valley for irrigation, partially filling the deepest sections of the Salton Basin and effectively creating the modern Salton Sea. The volume of the Salton Sea is a balance between evaporative losses to the atmosphere and freshwater input, which includes runoff from local agricultural activity. As water use efficiency improved in the

*Corresponding author address: Amato Evan, Scripps Institution of Oceanography, University of California, San Diego, 8622 Kennel Way, La Jolla, CA 92037.
E-mail: aevan@ucsd.edu

agricultural industry over the 20th century there was a resultant reduction in runoff, and water losses outpaced inputs, resulting in a shrinking Salton Sea. This drop in the Salton Sea's surface height is accelerating; as part of a 2003 Water Transfer Agreement, the Quantification Settlement Agreement (QSA), starting in 2018 the amount of freshwater flowing into the Salton is being dramatically reduced (QSA 2003). Some estimates suggest an eventual 40% reduction in freshwater input to the Salton (Cohen 2014).

Given the shallow nature of the Salton Sea, the subsequent drop in the height of the Sea will result in a large reduction in the Salton's surface area. A recent estimate suggested that at present, and relative to 2003, there has been an increase of 20,000 acres of exposed playa (IID 2018). From this same study, and assuming no systematic changes in water input to the Salton Sea, the estimated rate of additional playa exposure over the next five years (2018–2023) will be 5,500 acres per year, and that by 2045, when the Sea level stabilizes, there will be a total increase of 105,000 acres of exposed playa, also relative to 2003. This exposure of dry lakebed surfaces to the atmosphere may alter the composition of particular matter in the region (Frie et al. 2017), and increase dust emission from the playa, although the only study of this effect was inconclusive (Parajuli and Zender 2018). The floor of the Salton Basin consists of a layer of wet alluvial deposits that is thousands of feet deep (USDI/CRA 1974), and pesticide-laden runoff from agriculture has been a major source of freshwater input to the Salton Sea over the last 100 years (Schroeder et al. 2002). Thus, not only is newly exposed playa erodible (Buck et al. 2011; Sweeney et al. 2011), but this soil could contain high levels of toxic material (Frie et al. 2017).

The purpose of this paper is to use observations to characterize the meteorological processes responsible for major dust storms originating in the Salton Basin. Due to the shrinking of the Salton Sea efforts are underway to test methods to mitigate dust emitted from the newly exposed playa, including vegetation enhancement, surface roughening, and surface stabilization with magnesium chloride (IID 2016). Consequently, understanding of the meteorology of these storms will undoubtedly be helpful in determining the locations where these mitigation efforts will be most needed, or where the exposed playa may be most sensitive to aeolian erosion due to high winds and saltation bombardment from upstream emission. Furthermore, the Salton Basin is a closed topographic depression, and while such depressions are small sources of dust, when compared to major dust source regions like the Bodélé or Taklimakan, such depressions are globally widespread (Engelstaedter et al. 2003), and dust from closed depressions may represent 30% of emission globally (Ginoux et al. 2012). Consequently, knowledge gained regarding dust emission from the Salton Basin may be applicable to understanding dust storms in other regions of the world.

The remainder of this paper is organized as follows: In the Data and Methods Section I briefly describe the various data sets used in the study. In the Results Section I first describe the meteorology underlying a single dust outbreak that occurred on March 14, 2018. I then determine if these results can be generalized to understand the meteorology of the 10 largest dust outbreaks in the region during the period 2015–2018. This is followed by a more general look at the meteorological conditions associated with elevated surface PM_{10} concentrations. Lastly, in the Conclusions I summarize the main findings and discuss uncertainties in the analysis and the types of observations that are needed to address them.

2. Data and Methods

I utilize hourly averaged measurements of PM_{10} from stations maintained by the California Air Resources Board (CARB). CARB PM measurements were utilized for 2015–2018, as 2015 is the first calendar year for which PM measurements were made at 5 now permanent sites surrounding the Salton Sea (Fig 1b, filled circles). I also utilize hourly averaged measurements of surface wind speed U and direction from these same stations, and for the same time period. CARB data and detailed site and instrumentation information is available at https://www.arb.ca.gov/aqmis2/aqdselect.php. For the March 14, 2018 case study, additional surface measurements of wind speed and direction, and temperature were taken from the MesoWest network (Horel et al. 2002), https://mesowest.utah.edu. The locations of these surface stations are shown in Figure 1b (red, empty circles). Upper air measurements for the case study were from soundings made in San Diego, CA, and were accessed from the Wyoming Weather Web, http://weather.uwyo.edu/.

For the case study I also used imagery from a Roundshot 360^{o} camera that is managed by the Imperial Irrigation District (IID). The location of this camera is in Figure 1a. The panoramic imagery is available at approximately 20-minute intervals via https://iid.roundshot.com. A video of all images captured for arch 14, 2018 is available in the online Supplemental for this manuscript.

MODerate resolution Imaging Spectrometer (MODIS) true color and aerosol optical depth (AOD) imagery was used for the case study and the analysis of the 10 major dust outbreaks during the 2015–2018 time period. MODIS data was accessed via the NASA Worldview application (https://worldview.earthdata.nasa.gov/), which is operated by the NASA/Goddard Space Flight Center Earth Science Data and Information System (ESDIS) project. The MODIS AOD products include retrievals via the Deep Blue algorithm (Hsu et al. 2013).

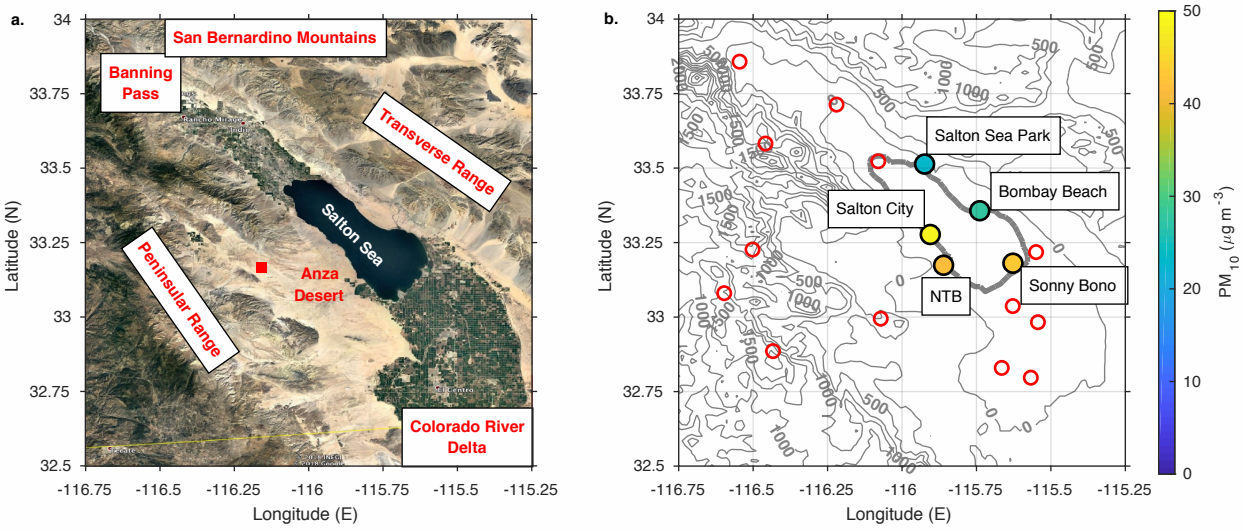

FIG. 1. Geography of the Salton Basin. Shown in 1a is an image of the region of interest, with the major topographic features labeled. The red square represents the location of an IID 360° RoundShot camera. Plotted in 1b are regional elevations contours (m), with the approximate shoreline of the Salton Sea represented by a thick gray line. Here, the red circles represent locations of surface stations where winds, temperature, and/or PM_{10} are measured, for the case study. The filled circles represent CARB sites measuring PM_{10} since at least January 2015, where colors correspond to mean PM_{10} values over 2015–2017. The names of these CARB sites are also indicated.

Lastly, output from the North American Regional Reanalysis (NARR, Mesinger et al. 2006) was used for the March 14, 2014 case study, and analysis of 10 major dust outbreaks in the region (Table 1). NARR is a high-resolution climate dataset for the North American domain, and 3-hourly output is available at a nominal 32 km horizontal resolution with 29 layers in the vertical from the NOAA/OAR/ESRL PSD (https://www.esrl.noaa.gov/psd/).

3. Results

In this section I present a case-study of a major dust outbreak that occurred in the Salton Basin on March 14, 2018. This particular event was chosen for analysis because 1) the dust storm was clearly visible in satellite imagery, 2) continuous wind and PM_{10} measurements were available for the sites indicated in Figure 1b, and 3) RoundShot camera imagery was available for that entire day. This case study is followed by an examination of the 10 largest dust events in the basin over the time period 2015–2018, as indicated by surface measurements of PM_{10} and satellite imagery, the purpose of which is to determine if the meteorological processes underlying most major dust outbreaks in the region are similar to that identified for the March 14 case.

a. March 14, 2018 Case Study

On the days immediately preceding and following the March 14, 2018 dust outbreak, there was a slow-moving upper level low over the northeastern Pacific. This upper low directed a series of surface lows through California, one of which passed through the state early in the morning of March 14. This particular storm produced rainfall and hail along the coast, and storm-total snowfall amounts greater than 80 cm in parts of the southern Sierra Mountains (from the NOAA National Centers for Environmental Information Storm Events Database, https://www.ncdc.noaa.gov/).

Reanalysis 300 hPa heights and streamlines, averaged over the 24-hour period ending at 1600 PST on March 14 , show the center of action of this upper level low at approximately 50°N and -135°E (Fig 2a). High wind speeds (e.g., greater than 45 m s^{-1}) are found mainly to the left of the negatively tilted trough axis (Fig 2a, shading), and are indicative of trough amplification. Flow around the trough is oriented perpendicular to the coastline south of 40°N, and thus perpendicular to the ridge of the Peninsular range (Fig 1a), and the downwind Salton Basin (red marker).

Reanalysis sea level pressure, also averaged over the 24-hour period ending at 1600 PST, shows a surface low centered at approximately 40°N and -117°E (Fig 2b, gray contours). The 850 hPa streamlines to the east of the region of interest (red square marker) turn clockwise over land, and here the corresponding 850 hPa wind speeds accelerate to values greater than 12 m

s^{-1} (shading), both of which are associated with a cold front passing through the region (frontal location determined from the Weather Prediction Center surface analysis, http://www.wpc.ncep.noaa.gov/html/sfc2.shtml, not shown).

1) EARLY MORNING CONDITIONS

A sounding made from San Diego at 0400 PST on March 14 (1200 UTC, station NKX at -117.12°E and 32.85°N, which is directly west of the red square marker in Figs 2ab) shows a moist marine layer from the surface to 780 hPa (Fig 3). The low-level saturated layer is capped by a shallow inversion, and then an isothermal layer from 770-700 hPa. Above 700 hPa, the atmosphere approximately follows a moist adiabat. The winds throughout the troposphere are westerly. Within the saturated layer the winds are between 5 kts (at 1000 hPa) and 20 kts (at 800 hPa), and above the inversion (600 hPa) the wind speeds jump to 40 kts, and steadily increase in magnitude with height thereafter. At the time of the sounding the surface wind speeds at met stations within the Peninsular mountains (at elevations above 1000 m) were 5-10 kts, and southwesterly to westerly (Fig 4), consistent with the sounding (Fig 3). Within the sub-sea level Salton Basin the winds were on the order of 5-10 kts and mainly westerly (Fig 4). The hourly mean PM_{10} measurements in the Basin and at this same time are 0.2-22.4 μgcm^{-3}, indicating a lack of dust in the atmosphere.

The slow wind speeds below the inversion in the 0400 PST sounding are indicative of flow blocking by the Peninsular Mountain Range. An east-west transect of surface elevation, averaged from 32.5 to 33.5°N, shows that the Peninsular Mountains rise from the coast to an average height of 1,200 m over less than 1° longitude, before falling down to the Salton Basin over a similar horizontal distance (Fig 5a). A north-south transect of the maximum heights in the Peninsular range shows that much of the range's ridge line is between 1,500 to 3,000 m in height (Fig 5b). The heights of the mountains approximately correspond to the height of the inversion and low wind speeds in the sounding (Fig 3), and thus are consistent with flow blocking by this range. Furthermore, from a MODIS-Terra image corresponding to an 1100 PST overpass (Fig 6a), the pattern of cloud cover is also suggestive of flow blocking; cloud cover is pervasive along the windward side of the Peninsular Range, while in the lee there are cloud bands oriented parallel to the mountain ridge line, indicating trapped lee waves.

Interestingly, at 0400 PST (Fig 4) there were strong (20 kts) westerly surface wind speeds at a site located in the town of El Centro (-115.7°E and 32.8 °N), which is 10 kts higher than the wind speeds measured further to the north in the Salton Basin. As will be shown in subsequent sections, as the winds increase in magnitude throughout the day, the wind speeds measured at the El Centro station remain higher than those measured further north in the Basin. It is plausible that the high wind speeds in El Centro are due to downslope acceleration of flow being channeled through the gap that lies to the south of Monument Peak, which I will refer to as the "El Centro Gap" in Figure 5b, and which is the lowest point (1170 m) in the north-south transect of the Peninsular Mountains. However, the winds are not associated with dust uplift, mainly because the surface to the east of the gap is very rocky with few emissive regions, and then quickly transitions to cropland (as evidenced by an *in-situ* examination of the landscape).

2) DUST EMISSION

The March 14, 2018 dust event began in the late morning hours. At 0850 PST, an image from the Anza desert Roundshot camera (location in Figs 1 and 6) shows good visibility to the south and to the east (Fig 7a), with distant mountain ranges and hills visible (blue arrows). In these images, direction is relative to the location of the camera (Fig 6), such that 90° is looking eastward from the camera location, and 180° is looking southward. By 0930 PST dust uplift is visible to the south and southeast of the camera (Fig 7b), and the leading edge of a dust front is apparent at a direction of 150° (red arrow). For reference, the hill indicated by the rightmost blue arrow is obscured by the dust. By 1020 PST the dust front identified at 150° (Fig 7b) has traveled eastward and is now at 120° (Fig 7c, red arrow). I note that Roundshot images for times between 0930 and 1020 LT are available, but not shown here for brevity. Dust emission is also seen east of the camera location, between the directions of 80 and 110°. In Figure 7c the mountains behind the lofted dust (leftmost blue arrow) are obscured, when compared to the image at 0930 LT (Fig 7b). At 1100 PST dust is still being emitted to from the land surfaces that lie to the east of the camera (Fig 7d). In addition, the hill to the south is completely obscure, indicating continued dust emission in this area as well, although the emission may be upwind (to the west) of this hill and then advected eastward. In general, by 1100 PST, much of the field of the camera's view, between 70° and 180°, is obscured by dust.

The dust plumes visible in the Roundshot imagery (Fig 7) are not easily seen in the 1100 PST MODIS-Terra image (Fig 6a), mainly because the suspended dust does not provide a good visual contrast against the desert surface. In this satellite image there are only faint traces of dust being advected over the Salton Sea. However, the corresponding PM_{10} measurements (Fig 8) show elevated values along the western shore of the Sea (131 and 51 $\mu g\ cm^{-3}$) and immediately to the south of the Sea (86 and 98 $\mu g\ cm^{-3}$), which constitute an increase compared to the

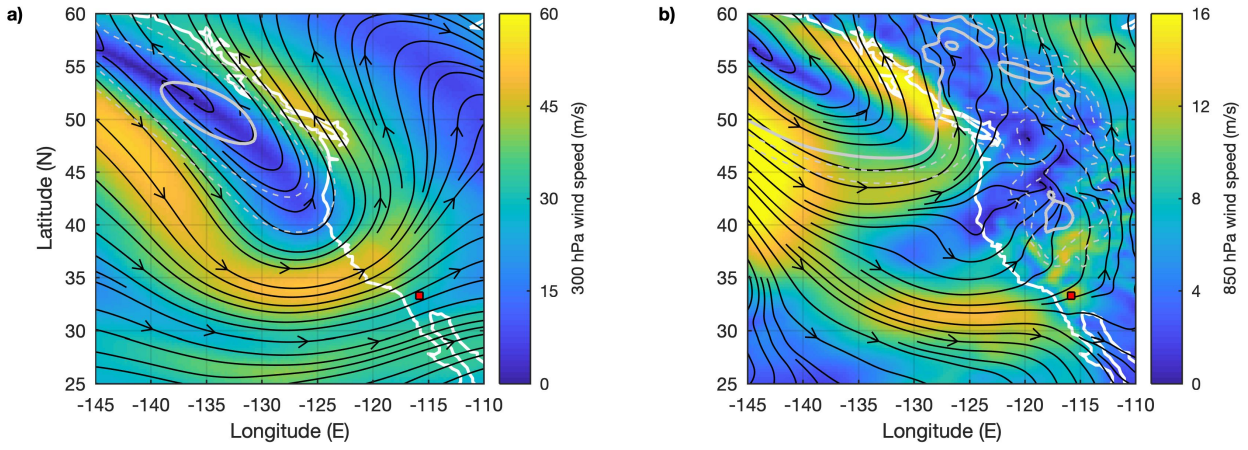

FIG. 2. Synoptic conditions associated with the March 14, 2018 dust outbreak. Shown in 2a are the 300 hPa wind speeds (shading), streamlines (black contours), and heights of the 300 hPa pressure surface (gray contours). The height contours correspond to 8800 m (solid), and 8850 and 9000 m (dashed). Shown in 2b are the 850 hPa wind speeds (shading), streamlines (black contours), and sea level pressure (gray contours). The isobars correspond to the 1006 hPa surface (solid), and the 1008 and 1010 hPa surfaces (dashed). All fields represent averages over the 24-hour period ending at 1600 PST on March 14. The red marker in each panel corresponds to the location of the Salton Basin. All meteorological data is from NARR.

early morning values (Fig 4). Also at 1100 PST, the station along the western shore of the Sea that measured the largest increase in PM_{10} (Salton City site in Fig 1b) also measured a mean westerly wind of 20 kt (Fig 8), which is an increase of 10 kts from 0400, and is consistent with the Roundshot imagery (Fig 7). The PM_{10} measurements along the northern coast of the Salton Sea remain near zero because the dust generated within the Anza desert is advected eastward. The exceptionally high value of 325 μg cm^{-3} at the station located at 33.3^{o} and -115.9^{o} was likely the result of either an instrument error or fugitive dust (*e.g.*, nearby passage of a vehicle on a dirt road).

Starting at approximately 1140 PST there is a large increase in the amount of dust being emitted within the Anza Desert (not shown), and at 1210 PST dust emission is visible in the foreground of the entire Roundshot scene from 80^{o} to 180^{o} (Fig 9a). This afternoon dust front is advected eastward, and by 1300 PST, PM_{10} values along the western and southern shoreline of the Salton Sea have increased to values ranging from 177 to greater than 250 μg cm^{-3}, and wind speeds along the southern half of the Sea are westerly at 20 kts (Fig 10). A true color image

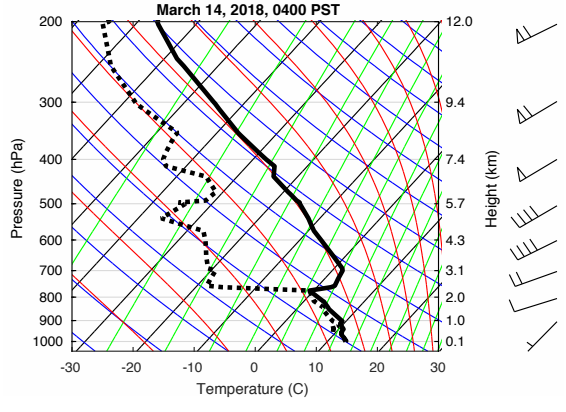

FIG. 3. Sounding from 1200 UTC (0400 PST) made at San Diego station NKX at -117.12^{o}E and 32.85^{o}N.

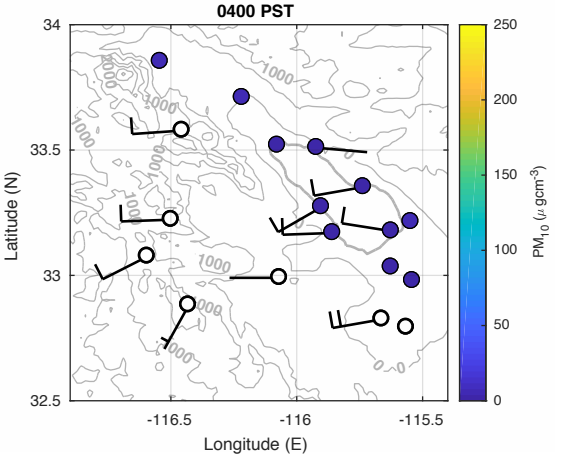

FIG. 4. Surface meteorological and PM_{10} observations at 0400 PST. Gray contours indicate surface elevation (at 500 m intervals), with the Salton Sea indicated by a slightly thicker contour. Shading reflects PM_{10} values at this time, with black indicating that no PM_{10} measurements are made at the site.

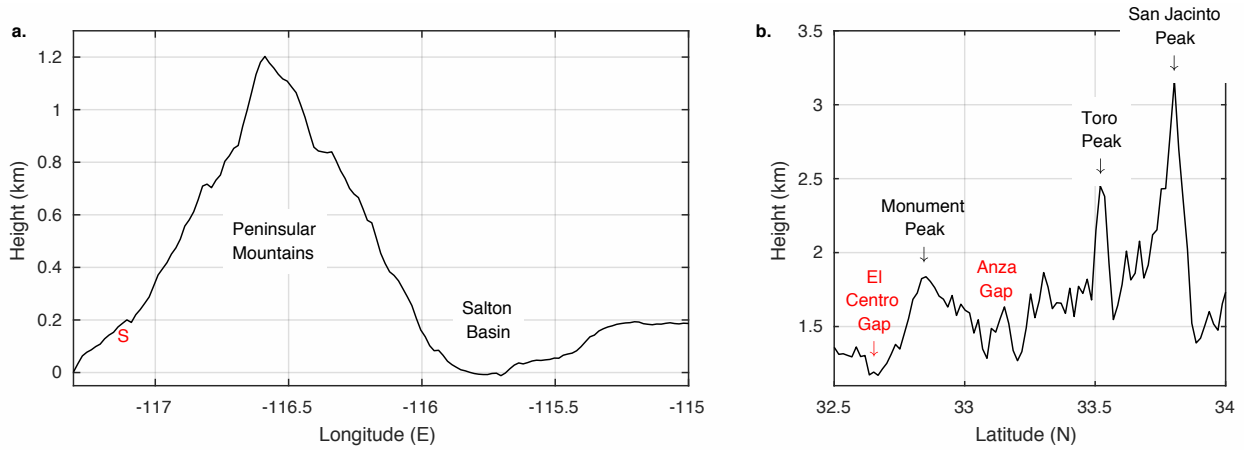

FIG. 5. Transects of the topography through the region of interest. Shown in 5a is an east-west transect of surface elevation (Fig 1b), averaged from 32.5-33.5°N. The coastline is at a longitude of approximately -117.3°E, and the longitude and heights of the NKX sounding station is indicated by the red "S". Shown in 5b is a north-south transect of the maximum surface elevations found between -117.5 and -116°E. Note that the heights are biased low (by approximately 200m for the mountain peaks) because of the elevation map horizontal resolution. The major peaks within the Peninsular Mountains are indicated, as are gaps in the elevation that are relevant to understanding dust outbreaks in the Salton Basin.

from the MODIS-Aqua satellite, corresponding to a 1235 PST overpass shows dust to the east and southeast of the IID Roundshot camera, including dust advected over the Salton Sea, and advected over the agricultural regions to the south of the Sea (Fig 6b).

From the Roundshot imagery, at 1310 PST there is less dust emission visible within the Anza Desert (Fig 9b), and the main wall of dust seen in the foreground of the 1210 PST image (Figs 9a) has propagated eastward and away from the camera location. By 1620 PST there is no obvious dust emission from the desert, although dust is still visible in the distance (Fig 9c). By 2000 PST, PM_{10} values and wind speeds within the Salton Basin have dropped back to the values observed at 0400 PST (Fig 4, 2000 PST measurements not shown).

3) DOWNSLOPE WINDS AND HYDRAULIC JUMPS

Based on the coincident measurements of PM_{10}, and wind speed and direction, the dust event on March 14, 2018 was due to accelerated westerly flow at the surface (Figs 8 & 10), and it is likely that these strong westerly winds were the result of a lee side downslope windstorm and hydraulic jump. Initiation of dust events by downslope winds has been shown to be the fundamental mechanism for producing exceptionally large dust storms in Owens Valley, California (e.g. Jiang et al. 2011), which lies approximately 300 miles north of the Salton Basin. Other recent studies have suggested that downslope acceleration of the surface flow is an important mechanisms for dust uplift over the Sahara (Gläser et al. 2012; Pokharel et al. 2017).

I firstly evaluate the hypothesis, that the high wind speeds along the floor of the Salton Basin were due to a downslope windstorm, by evaluating the so-called flow regime for this case, via examination of the shallow water Froude number F and the non-dimensional mountain height M (Houghton and Kasahara 1968). The shallow water Froude number F is given by

$$F = \frac{U}{\sqrt{g'H}}$$

where U and H are the wind speed and layer depth, respectively, of the upstream unperturbed flow, and g' is the reduced gravity (Long 1954; Vosper 2004),

$$g' = g\frac{\Delta\theta}{\theta_o}$$

where g is gravitation acceleration, θ_o is the potential temperature at the base of the inversion layer (800 hPa in Figure 3) and $\Delta\theta$ is the potential temperature difference from the inversion base to its top (at 800 hPa). The non-dimensional mountain height M is defined as

$$M = \frac{h_m}{H}$$

where h_m is the physical height of the obstruction, which in this case is the height of the Peninsular Range.

Based on the 0400 PST sounding from San Diego (Fig 3), I estimate $U = 20$ ms^{-1}, and $H = 3{,}000$ m, which are the wind speed and height, respectively, at the top of the low-level inversion (approximately 700 hPa). According to the sounding, the potential temperature at the base of the inversion is 295 K, and $\Delta\theta$ is 11 K, such that $g' = 0.37$

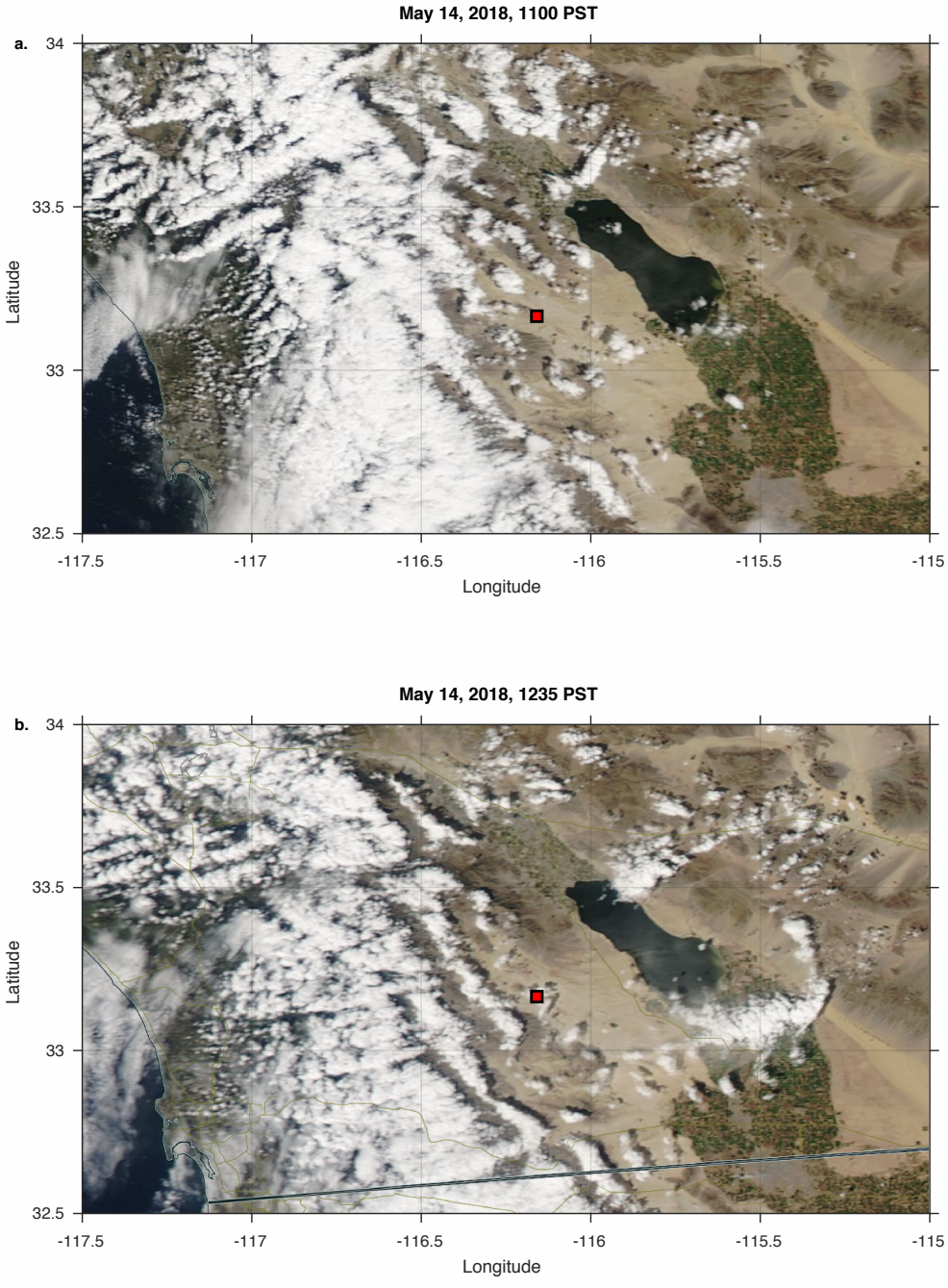

FIG. 6. True color images for March 14, 2018 of the regions of interest, created from the MODIS instruments flying onboard the Terra (a) and Aqua (b) satellites. Satellite overpass times (PST) are indicated in the image titles. The red square indicates the locations of the Anza Desert IID Roundshot camera. MODIS imagery from NASA Worldview (worldview.earthdata.nasa.gov).

m s^{-1} I also assume that $h_m = 1{,}500$ m, since this is the average height through the Anza Gap (Fig 5b). Thus, $F = 0.60$ and $M = 0.5$. Making minor but reasonable changes in the parameters used to calculate F and M resulted in qualitatively similar results.

From Houghton and Kasahara (1968, their Figure 3), these values of F and M are consistent with a nonlinear flow regime consisting of a lee side hydraulic jump. As implied with $F < 1$, the upstream flow is blocked and the maximum wind speed is on the downslope side of the ob-

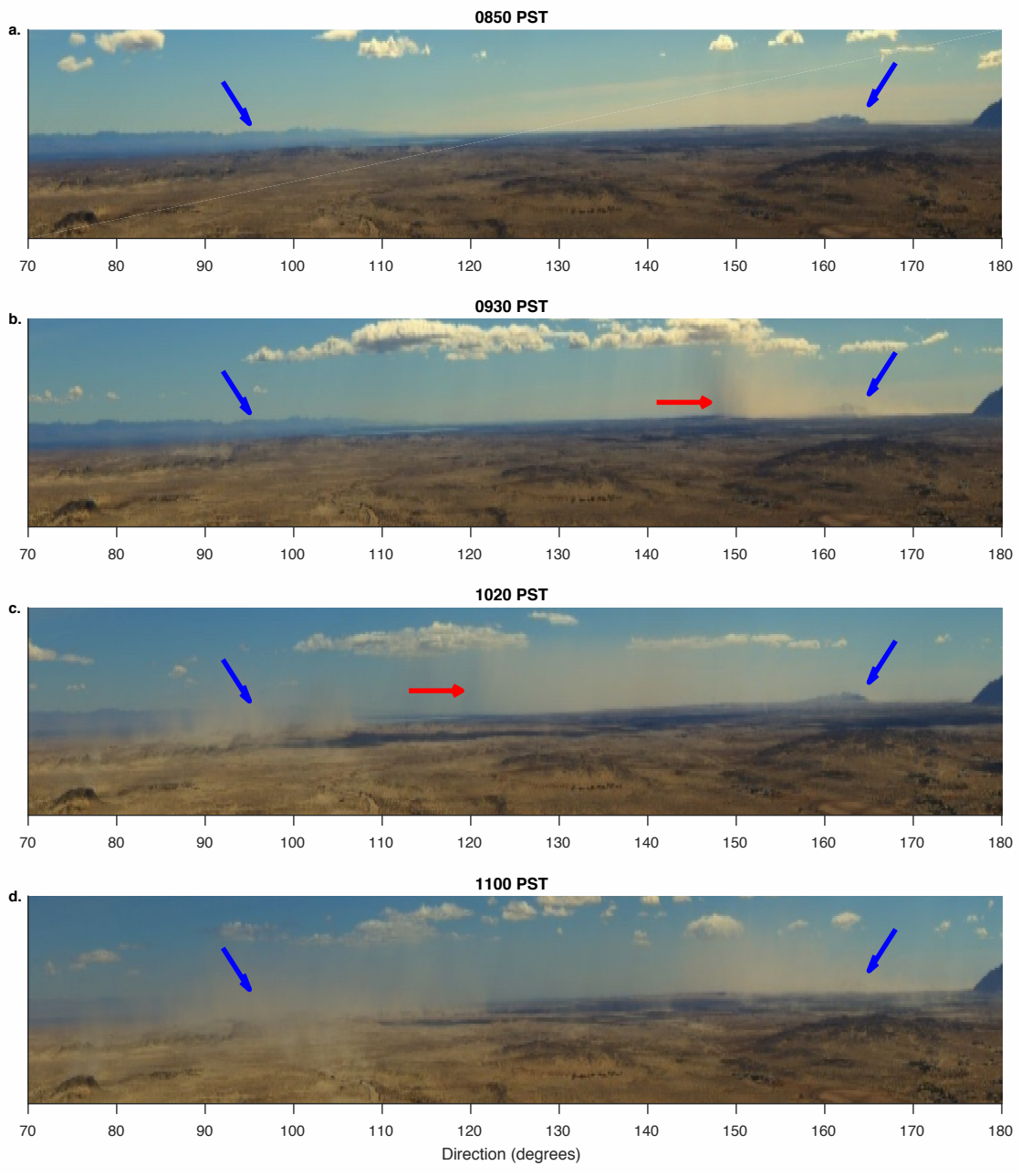

FIG. 7. Shown are four images from the IID Roundshot camera located in the Anza Desert (Fig 1), taken at 0850 (7a), 0930 (7b), 1020 (7c), and 1100 PST (7c). The direction of view is indicate on the abscissa, where 0^o is north, 90^o is east, etc... The blue arrows points to reference hills that, throughout the image sequence, becomes obscured by suspended dust. The red arrow in 7b and c indicate the movement of leading edge of an individual dust front.

struction, which is a result of the conversion of upstream potential energy into lee side kinetic energy (Lin 2007, Chpt. 3). It is not clear if the lee side hydraulic jump is stationary or transient, since these values of F and M suggest a near zero jump propagation velocity (Houghton and Kasahara 1968).

From the IID Roundshot imagery, the dust appears as a vertical front, including the propagating front from the morning images (Figs 7bc, blue arrows on righthand side of images), and what appears to be a stationary front in the afternoon images (starting with Figs 7d, 9a), which then slowly propagates to the east (Figs 9bc). The struc-

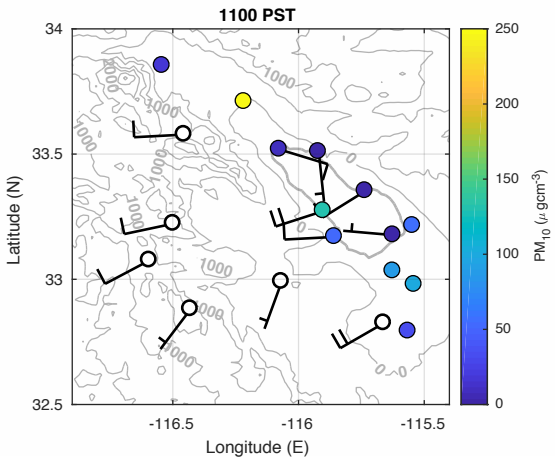

FIG. 8. Description is the same as for figure 4, except that the winds and PM_{10} observations correspond to 1200 LT.

ture of the lofted dust in these images is similar to that of downslope-windstorm and hydraulic jump generated dust events in the Owens Valley (e.g., Figure 6 in Jiang et al. 2011), and thus are consistent with the analysis of the flow regime. Additionally, in the satellite imagery for this day (Fig 6), there is a reduction in the cloud cover, or a foehn gap, in the lee of the Peninsular Range, particularly over the Anza desert, where the dust emission is occurring.

4) DOWNSLOPE WIND PENETRATION DEPTH

I next examine the timing of the dust emission initiation and termination. In Owens Valley it was shown that stably stratified westerly winds aloft would descend dry adiabatically in lee of the Sierras, but only to a depth for which the density of the downslope flow was greater than that of the ambient air (Mayr and Armi 2010; Armi and Mayr 2011). Consequently, emission of dust would only commence when the temperature of the air at the Valley floor was greater than the potential temperature of the air spilling over the ridges of the Sierras. Similarly, emission would terminate once the temperature of the air at the Valley floor dropped below the potential temperature of the air at the ridges.

Similar to the case of the Owens Valley, the timing of the March 14, 2018 dust event in the Salton Basin may have been due to the density differences between the descending air mass and the air at the base of the Salton Basin. I evaluate this hypothesis by comparing temperatures measured near Monument Peak in the Peninsular Range (Fig 5), with those measured at Salton City (Fig 1b), which is downwind of the Anza Desert and along the western shore of the Sea. The mountain station, indicated as "Mt. Laguna" (32.88°N, -116.43°E) is at an elevation of 1,812 m, while the Salton City station is at 61 m below sea level. Thus, assuming that air flowing over the Peninsular mountains is descending adiabatically to the Basin floor, we compare the *in-situ* temperature measured at Salton City with those from Mount Laguna plus an offset value of 18.7 C, which represents the warming of the descending flow (1870 m $\times$ 10 C km^{-1} lapse rate).

A time series of hourly mean temperature at Salton City (Fig 11a, red), shows a morning minimum of 19.5 C at 0600 PST and a maximum of 25.5 C during 1100 and 1200 PST. The hourly time series for temperature plus the 18.7 C offset for Mt. Laguna (Fig 11a, blue) has a maximum of 26 C at the beginning of the day, and minimums or 20 C at 2000 and 2200 PST. From this figure, the Laguna temperature is greater than that from Salton City through 0900 PST, suggesting that air descending in the lee of the Peninsular range would not penetrate to the Basin floor during this time. However, between 0900 and 1000 PST the temperatures at Salton City become greater than the Mt. Laguna temperature (plus 18.7 C offset), possibly due to cooling at Mt Laguna associated with cold front passage, and warming at Salton City from solar heating at the surface. The temperatures at Salton City remains greater than that of the flow descending in the lee of the range until 1800 PST, suggesting that after this time air descending over the lee of the range will no longer be sufficiently dense to penetrate to the Basin floor.

A time series of wind speed at Salton City shows wind speeds in the range of 3 to 7.5 m s^{-1} through 0900 PST (Fig 11b, red). Consistent with the crossing of the two temperature time series in Figure 11a, after 0900 PST wind speeds rise rapidly to 13.5 m s^{-1} between 1000 and 1300 PST, stay above 12 m s^{-1} through 1700 PST, and begin to drop rapidly at 1800 PST. The rapid increase and decrease in wind speeds in Salton City approximately corresponds to the crossing of the Salton City and Mt. Laguna temperatures at 0900 and 1800 PST, and thus is consistent with a downslope windstorm and the the theory of the timing of the winds based on density differences (Mayr and Armi 2010; Armi and Mayr 2011). This is also consistent with the timing when dust appears in the 0930 PST Roundshot imagery (Fig 7a), and when dust is no longer visible in the scene (2000 PST Roundshot imagery, not shown). Hourly wind speeds at the Mt. Laguna site (Fig 11b, blue) show little variation throughout the day, are only in the range of 2-4.5 m s^{-1}.

Lastly, a longitude-height transect of NARR potential temperature, averaged from 32.5–33.5°N latitude, indicates flow blocking on the windward side of the Peninsular range, where isentropes less than 292 K terminate below heights of 1000 m (gray contours, Fig 12) and zonal wind speeds are under 9 m s^{-1} (shading). In the lee of the range there is isentropic folding between 1000 and 2000 m, with a superadiabatic lapse rate between 1000 and 1500 m, and associated generation of turbulent kinetic energy at these same heights (black dotted contours, Fig 12). These features in the reanalysis are consistent with isentropic draw-

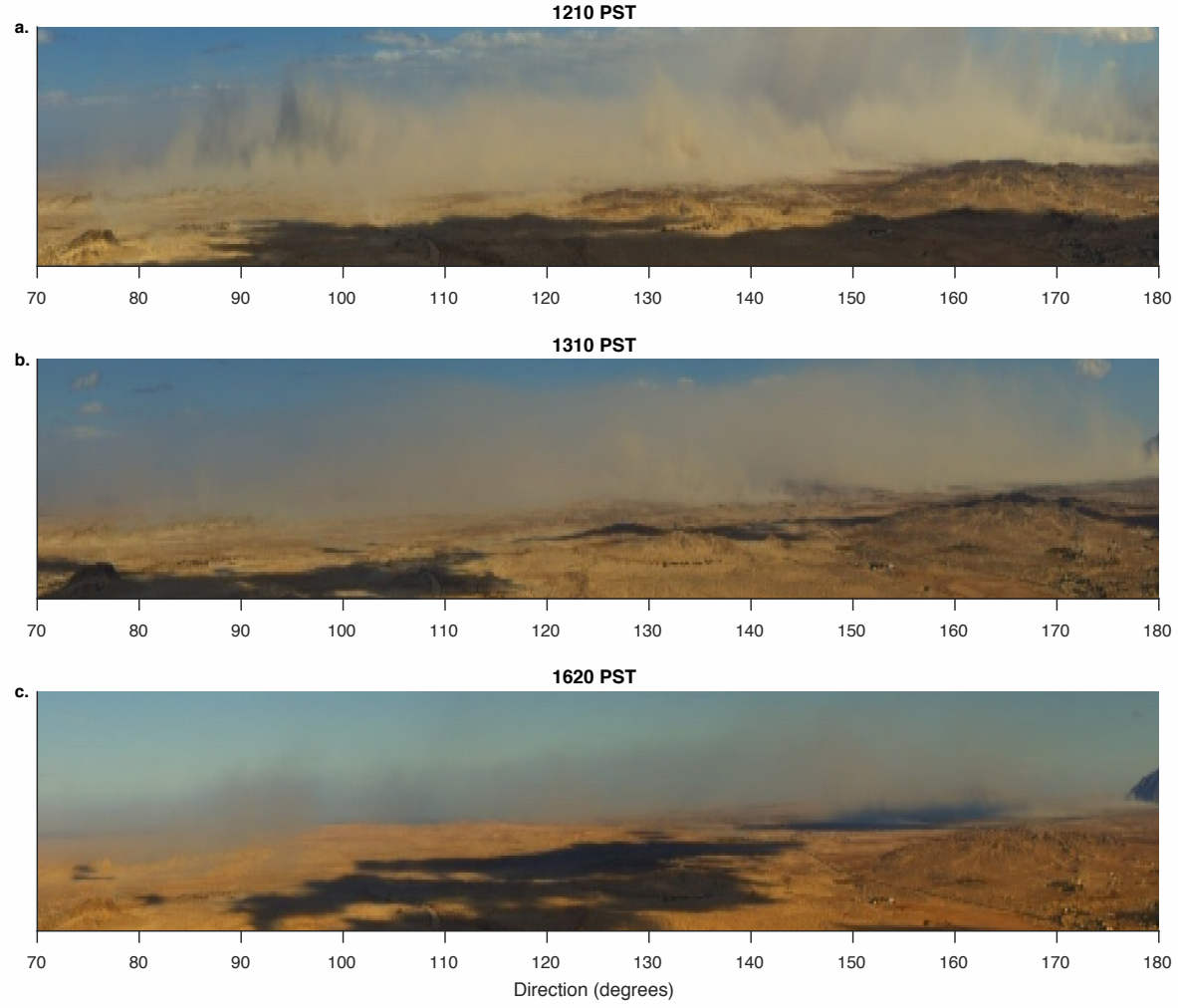

FIG. 9. Description is the same as for Figure 7 except that images correspond to different times.

down in the lee of the mountains and downslope flow acceleration, and are consistent with a study of downslope winds and dust generation in the Sahara (Pokharel et al. 2017).

In Figure 12, the surface wind speeds in the lee of the range only accelerate to mid-way down the mountain slope, with a maximum speed of approximately 12 m s^{-1} at a height of 500 m (approximately -116.2ºE), and similar plots for subsequent hours share this same feature. Analysis of NARR surface wind speeds in the region of dust emission show no increase in surface wind speed throughout the day (not shown). Thus, the lack of high lee-side wind speeds below heights of 500 m may be the result of a limitation in the reanalysis model, or the coarseness of the reanalysis output, which would be consistent with Pokharel et al. (2017), who demonstrated that a high-resolution mesoscale model was needed to reproduce the relevant features of dust-generating terrain-induced flow.

b. Discussion

The case study of the March 14, 2018 dust outbreak suggested that a westerly downslope windstorm was the main mechanism responsible for the dust uplift in the Anza desert, and transport eastward across the Salton Basin, and that this downslope windstorm may have been accompanied by a hydraulic jump in the lee of the range. But how common are dust storms generated via this mechanism? In order to address this question I examine the meteorology of the 10 largest dust events from 2015–2018 (Table 1), which includes this case study. These dust events were identified as those having the 10 highest values of daily mean PM_{10} for which suspended dust could be clearly identified in satellite imagery. I only considered cases where dust was visible in satellite imagery in order to conclude that the high PM_{10} values were indeed due to emitted dust, as opposed to erroneous measurements

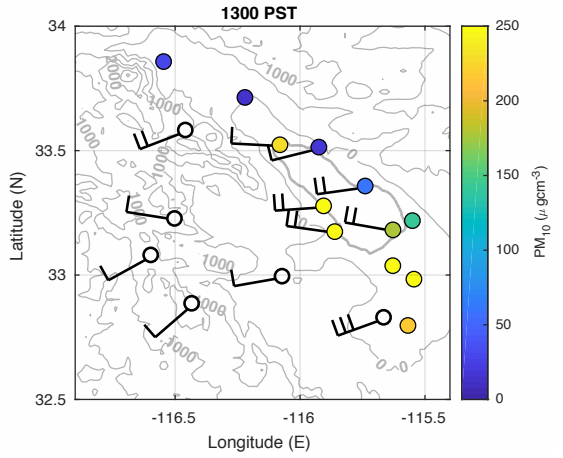

FIG. 10. Description is the same as for figure 4, except that the winds and PM_{10} observations correspond to 1300 PST.

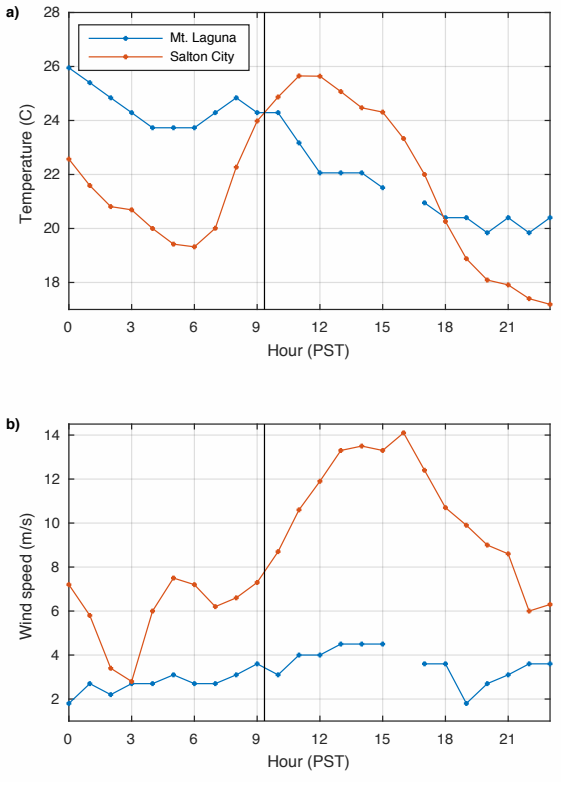

FIG. 11. Hourly temperature and wind speed at Salton City and Mt. Laguna on March 14, 2018. Plotted in 11a are hourly time series of temperature measured at Salton City, and temperature measured at Mt. Laguna plus an offset value of 18.7 C that accounts for dry adiabatic descent of air from 1870 m (elevation of the Mt. Laguna station) to -60 m (elevation of the Salton City station). Shown in 11b are hourly time series of wind speeds measured at these two sites.

or fugitive dust, which constituted 14 other cases. Thus, these dust events are those that occurred during the daytime and under clear-sky, or partially clear-sky conditions.

In Table 1 all vales of PM_{10}, and wind speed and direction, are averages over the five stations indicated in Figure 1b. For these 10 dust events, the daily averaged PM_{10} ranges from 300-962 μg m^{-3}. The daily maximum wind speeds fall between 12.0 and 17.7 m s^{-1}, values that are above the 90th percentile of daily maximum wind speeds during 2015–2018 (11.8 m s^{-1}). The average wind directions, which correspond to the hour of the daily maximum wind speed, are between 234 and 270 degrees, or southwesterly to westerly. Thus, these major dust events all are associated with anomalously strong westerly flow.

Date	PM_{10} (μg m^{-3})	Wind speed (m s^{-1})	Wind direction (deg)
2018/04/19	300	12.0	262
2018/03/14	**320**	**14.1**	**256**
2018/05/11	394	14.0	258
2016/03/06	489	15.3	269
2017/06/11	530	15.7	251
2016/04/25	535	16.6	270
2018/11/29	578	12.8	234
2016/12/16	679	17.7	248
2018/04/16	952	15.8	241
2017/10/20	962	14.6	262
Average	**582**	**14.9**	**255**

TABLE 1. Dates, maximum PM_{10}, maximum wind speed, and corresponding wind direction, for the 10 large dust events in the Salton Basin for 2015–2018 (case study in bold). All data is based on averages of measurements from the five stations indicated in Figure 1b. The wind speed is the maximum hourly averaged (over the five stations) wind speed for the indicated day. The wind direction is the measured direction, averaged over the five sites, at the time of the maximum wind speeds.

Are the synoptic conditions associated with the March 14, 2018 case study (Fig 2) representative of major dust outbreaks in the region? A composite map of reanalysis heights and streamlines at 300 hPa, averaged over the 24-hours ending at 1600 PST on the day of the emission event, and averaged over the 10 events in Table 1 (Fig 13a), show an upper level low (gray contours) with its center of action at approximately 45°N and -125°E, and a trough axis oriented parallel to the coastline (black lines). High wind speeds of approximately 35 m s^{-1} (shading) to the left of the trough suggest trough amplification prior to the emission events.

A composite map of the daily mean streamlines at 850 hPa, also averaged over the 10 events in Table 1, includes an offshore northwesterly low-level jet that turns zonal as it crosses the coastline between 30 and 35°N (Fig 13b). Similar to the case study (Fig 2b), over land the jet con-

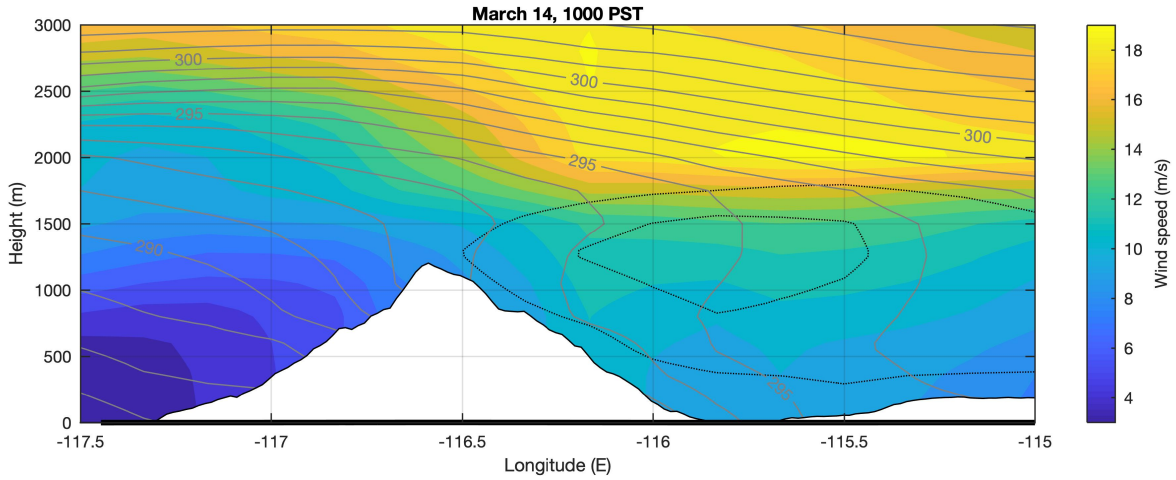

FIG. 12. Longitude height cross section at 1000 PST on March 14, averaged over 32.5–33.5°N latitude. The filled contours represent zonal wind speed (m s^{-1}), the gray contour lines are isentropes in increments of 1 K, and the dotted black lines represent the 5 and 10 J kg^{-1} isopleths of turbulent kinetic energy. All data is from NARR.

tinues a counterclockwise rotation, where wind speeds are greater than 10 m s^{-1} up to 40°N, directly below the 300 hPa jet exit region (Fig 13a). A composite of sea level pressure shows a surface low of 1004 hPa over the interior (gray contour, Fig 13b), and thus the southerly flow to the south of this low pressure center, and the coincident strong 850 hPa wind speeds, are consistent with cold frontal passage.

The composite maps of 300 and 850 hPa streamlines and wind speeds, and sea level pressure (Fig 13) are very similar to that shown for the case study (Fig 2). Thus, the synoptic conditions associated with the March 14 case study appear to be representative of conditions for the major dust outbreaks, with the key features being an upper level trough with its axis oriented along the coastline and it's center of action near 50°N, a surface low near 40°N and -115°E, and an associated prefrontal jet that is strongly zonally over the region of interest.

Next, is there evidence of downslope windstorms being an important mesoscale feature of the dust events in Table 1? To address this question I reproduce the time series of temperature and wind speed for the Mt. Laguna and Salton City stations (Fig 11), but averaged over these 10 events. In Figure 14a is an hourly time series of temperature at the Salton City station (red) and temperature at the Mt. Laguna station plus an offset of 18.7 C to account for adiabatic warming of this air descending 1870 m to the Basin floor (blue). These two temperatures first cross at 1130 PST (0930 PST in the case study), and at this time wind speeds at the Salton City site begin to rise rapidly, from values between 6-8 m s^{-1} between 0000 and 1000 PST, to a maximum of 12 m s^{-1} at 1500 PST (Fig 14b, red). At 1930 PST the temperature again cross, indicating that air descending in the lee of the Peninsular Range would no longer be sufficiently dense to reach the Basin floor (Fig 14a), and starting at 1800 PST the wind speeds at Salton City also begin to decline (Fig 14b). Wind speeds at the Mt. Laguna station remain between 2.5-4 m s^{-1} throughout the 24-hr period. Excluding the March 14, 2018 date for the composite analysis resulted in nearly identical results.

The hourly time series of temperature and wind speed, averaged over the 10 dust events in Table 1 (Fig 14), are consistent with those for the March 14 case study (Fig 11). Thus, another condition for large dust events in the Salton Basin appears to be sufficient cooling of the air flowing over the Peninsular range, and/or warming of the air at the Basin floor, such that the overflowing air is sufficiently dense to penetrate to the Basin floor, and emit dust. However, based on the limited available data, an alternative hypothesis is plausible; afternoon dust emission is due to deepening of the desert boundary layer from dry convection initiated by strong surface solar insolation, and subsequent downward mixing of momentum from the free troposphere, a scenario observed in other dust-emitting regions (e.g., Marsham et al. 2008).

I note that excluding the March 14, 2018 date from the composite analysis at 300 and 850 hPa (Fig 13), and from the composite time series of surface properties (Fig 14), resulted in nearly identical results. Furthermore, for the analysis of the 10 largest dust outbreaks (Table 1) I only considered cases where PM_{10} was high and where dust was clearly discernible in visible satellite imagery (e.g., Fig 6). However, there were 14 other cases where PM_{10} was high, but the scene was completely obstructed by cloud cover, or where there was no dust visible in the

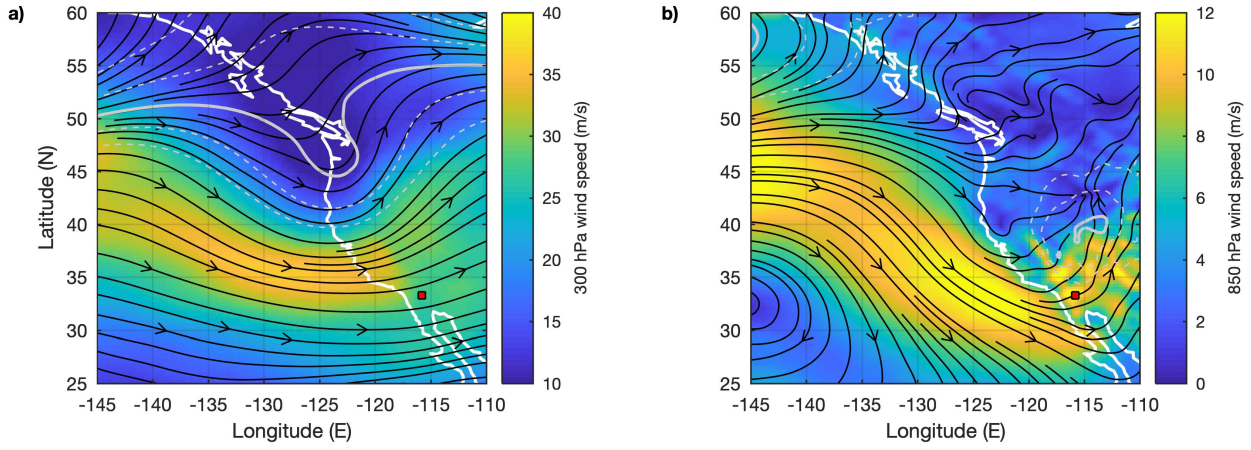

FIG. 13. Composites of synoptic conditions associated with the ten largest dust outbreaks in the Salton Basin over the period 2015–2018 (Table 1. Description is the same as for Figure 2, except that in 13a the heights of the 300 hPa pressure surface correspond to 9000 m (solid contour), increasing and decreasing heights in increments of 50 m (dashed contours), and in 13b the sea level pressure isobars correspond to 1004 hPa (solid contour), and 1006 and 1008 hPa (dashed contours). All data is from NARR

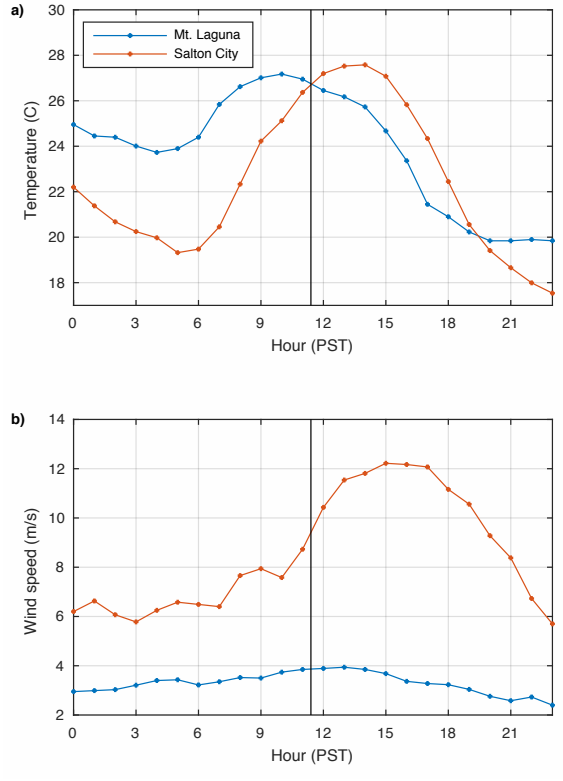

FIG. 14. Hourly temperatures and wind speeds measured at two sites during days with major dust outbreaks. Description is the same as for Figure 11 except that the hourly temperature and wind speeds correspond to averages over the 10 dust events indicated in Table 1.

clear sky scenes. For these cases I cannot discount the possibility that there were large dust events in the Basin, but that they simply were not apparent via the available satellite imagery, a situation which has been demonstrated further north in the Mojave (Urban et al. 2018).

Another way to determine if the characteristics of the ten dust events in Table 1 are more broadly representative is to evaluate wind speed and direction at the five stations surrounding the Salton Sea during all periods of elevated PM_{10}. In Figure 15a are wind rose diagrams corresponding to wind speeds when PM_{10} measured at the respective station is greater than the 95^{th} percentile of PM_{10} for that station, over the 2015–2018 time period. However, in order to avoid biases related to sampling of the diurnal cycle, these data only correspond to hourly PM_{10} and wind speed measurements for 1800 PST. This time of day was used because the climatological diurnal cycle of PM_{10}, averaged over the five sites in Figure 15a, is a maximum at 1800 PST (not shown), which is distinct from the March 14 case study where PM_{10}, averaged over the five sites, is a maximum from 1300-1600 PST (not shown).

In general, during high PM_{10} conditions, the wind directions at all stations except for Salton Sea Park are westerly or southwesterly, and wind speeds are greater than 10 m s^{-1} (Fig 15a), which is consistent with the case study (Fig 10), and the analysis of the 10 dust events (Table 1). The 1800 PST climatological wind speeds show that the highest wind speeds for all days in the record are between 10 and 15 m s^{-1}, and are also westerly (Fig 15b), again except for the northernmost station of Salton Sea Park. Thus, from a climatological perspective, the highest wind speed events in the basin are those responsible for generating dust storms there.

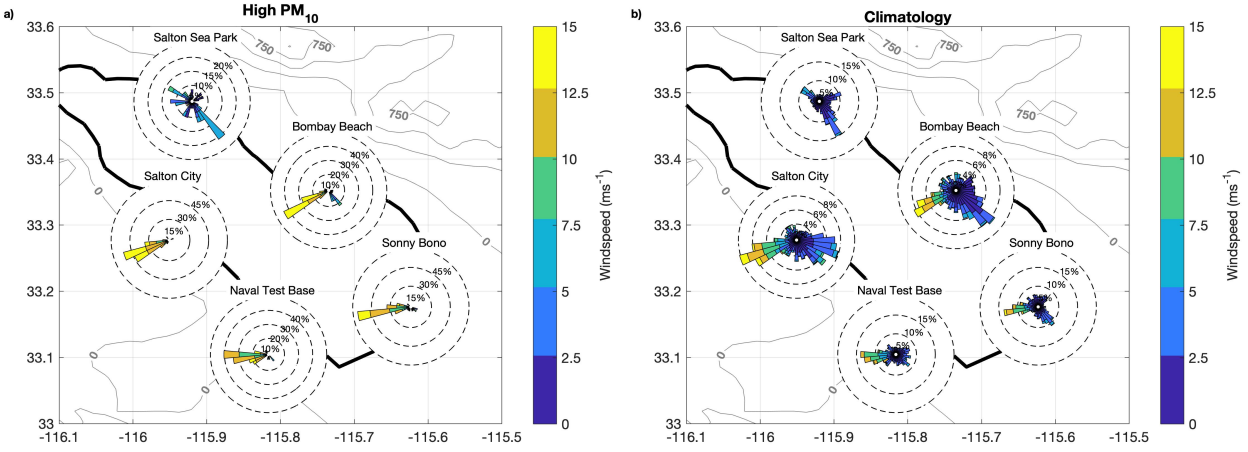

FIG. 15. Wind rose diagrams for stations around the Salton Sea at 1800 PST. Plotted in 15a are wind roses corresponding to times when the hourly PM_{10} values were above the $95^{th}\%$ of all PM_{10} values at 1800 PST, per station. Plotted in 15b are wind roses for all station data, at 1800 PST. The thick black contour represents the outline of the Salton Sea shoreline and the thin contours are surface heights (m).

Lastly, the northernmost station of Salton Sea Park is very distinct from the other four sites, where wind speeds are approximately half those at the other stations, and wind directions that are more southerly or northerly. It is likely that this station does not experience high wind speeds associated with westerly downslope wind storms as this stations lies to the north of the Anza desert, and is in a section of the basin that is very narrow (in the east-west direction) relative to the other stations (Figs 1ab). Consequently, the winds at this site may be more consistent with up- and down-valley flows.

4. Conclusions

In this paper I first presented an analysis of a single dust event in the Salton Basin. The main finding from this analysis is that an upper level low over the northeastern Pacific Ocean directed a zonal low-level jet over the region, and flow blocking by the Peninsular Mountain Range resulted in air from this jet descending in the lee of the range and penetrating down to the Basin floor. Starting in the late morning hours, these high wind speeds at the desert floor generated dust emission, which persisted until the mid-afternoon hours. Analysis of the ten strongest dust events, over the time period 2015–2018, suggested that these dust events shared consistent features with the March 14 case, including an upper level low that directs a low-level jet over the region of interest, temperature differences between air at height and air at the basin floor that are consistent with the timing of the build up of high wind speeds, and strong and westerly to southwesterly flow at the surface. Furthermore, a composite analysis of all available data suggested that the main features associated with Salton Basin dust storms are westerly and high wind speeds at the Basin floor.

The evidence suggesting that downslope windstorms are the main mechanisms responsible for dust-generating winds within the Salton Basin is still not conclusive. As such, one cannot rule out other plausible mechanisms, specifically downward mixing of higher momentum air in the free troposphere, due to solar insolation and deep dry convection over the desert surface (Marsham et al. 2008), a process that has been observed to be initiate dust outbreaks in the Sahara (e.g., Todd et al. 2013). Additional measurements in the lee of the Peninsular Mountains would be valuable to more conclusively understand the relevant physical processes, specifically measurements of upper atmosphere wind and temperature, boundary layer height, and the vertical structure of the emitted dust.

It is worth pointing out that the Anza Gap (Fig 5b) is the second lowest gap in the range, and is directly upwind of the Anza Desert. Thus, not only does this gap represents a natural location for air to descend in the lee of the Peninsular mountains, but the proximity of the desert means that this descending air, when sufficiently fast, is likely to result in dust uplift. This combination of orography and location of deflatable material at the surface is likely the reason why the basin experiences a high number of dust emission events, and high long-term mean PM_{10}, similar to other regions with frequent dust storms (Washington and Todd 2005; Washington et al. 2006b,a). Furthermore, as the north-south transect of the ridge line is not homogeneous (Fig 5b), one would not necessarily expect that the penetration of downslope winds to the Basin floor would be instantaneous in time. Thus, wind speeds

may build up rapidly over several hours, rather than arrive as a single front.

As discussed in the Introduction, dust emitted from small closed basins like the Salton may represent 30% of planetary dust emission (Ginoux et al. 2012). Climate models appear to struggle to reproduce many basic features of the dust cycle, at least over the Sahara Desert (Huneeus et al. 2011; Evan et al. 2014), and it is possible that the representation of surface wind speed variability is one reason for this deficiency (Evan 2018). Thus, by understanding the physical processes underlying emission in closed basins, it will be possible to evaluate these meteorological processes in climate models, with the goal of improving the representation of the dust cycle there.

Additionally, these results are regionally important as the Salton Sea is shrinking in surface area due implementation of a multi-state water transfer agreement (QSA 2003), and it is not entirely clear how future dust emission and regional air quality here will change (Parajuli and Zender 2018). During the 2015–2018 time period, long-term mean PM_{10} concentrations at the five CARB stations ringing the Salton Sea range from 25-50 μg cm^{-3}, values that exceed the California annual average allowable limit of 20 μg cm^{-3}. As such, a future increase in PM_{10} concentrations will likely exacerbate the associated negative human health consequences. Consequently, these results may also be useful in terms of evaluating and improving forecasts of winds and air quality within the Basin, and determining the most effective locations for dust mitigation activities within the drying seabed. Based on these results alone, dust emission from the drying lakebed may be most severe in the southwestern and southern (receding) coastlines of the Salton Sea. Firstly because wind speeds are exceptionally high in these areas. Secondly because these regions are also downwind of the dust blowing off of the Anza desert, and thus the dry playa surfaces will be bombarded by upwind emitted particles, which will have the effect of making these dry playa surfaces more susceptible to aeolian erosion (Bullard et al. 2011).

Acknowledgments. The author would like to thank three anonymous reviewers for their helpful comments on an earlier version of this manuscript. The author also acknowledges Laurence Armi, Leah Campbell, and Earl Withycombe for sharing their insights during the early stages of this work. Funding for this work was provided by NSF grant AGS-1833173.

References

Armi, L., and G. J. Mayr, 2011: The descending stratified flow and internal hydraulic jump in the lee of the sierras. *Journal of Applied Meteorology and Climatology*, **50 (10)**, 1995–2011.

Babcock, E. A., 1974: Geology of the northeast margin of the salton trough, salton sea, california. *Geological Society of America Bulletin*, **85 (3)**, 321–332.

Buck, B. J., J. King, and V. Etyemezian, 2011: Effects of salt mineralogy on dust emissions, salton sea, california. *Soil Science Society of America Journal*, **75 (5)**, 1971–1985.

Bullard, J. E., S. P. Harrison, M. C. Baddock, N. Drake, T. E. Gill, G. McTainsh, and Y. Sun, 2011: Preferential dust sources: A geomorphological classification designed for use in global dust-cycle models. *Journal of Geophysical Research: Earth Surface*, **116 (F4)**.

Cohen, M. J., 2014: *Hazard's Toll: The Costs of Inaction at the Salton Sea*. Pacific Institute.

District, I. I., 2016: Salton sea air quality mitigation program. Tech. rep., Formation Environmental, LLC, Air Sciences Inc., PlanTierra LLC.

Engelstaedter, S., K. Kohfeld, I. Tegen, and S. Harrison, 2003: Controls of dust emissions by vegetation and topographic depressions: An evaluation using dust storm frequency data. *Geophysical Research Letters*, **30 (6)**.

Evan, A. T., 2018: Surface winds and dust biases in climate models. *Geophysical Research Letters*.

Evan, A. T., C. Flamant, S. Fiedler, and O. Doherty, 2014: An analysis of aeolian dust in climate models. *Geophysical Research Letters*, **41 (16)**, 5996–6001.

Frie, A. L., J. H. Dingle, S. C. Ying, and R. Bahreini, 2017: The effect of a receding saline lake (the salton sea) on airborne particulate matter composition. *Environmental science & technology*, **51 (15)**, 8283–8292.

Ginoux, P., J. M. Prospero, T. E. Gill, N. C. Hsu, and M. Zhao, 2012: Global-scale attribution of anthropogenic and natural dust sources and their emission rates based on modis deep blue aerosol products. *Reviews of Geophysics*, **50 (3)**.

Gläser, G., P. Knippertz, and B. Heinold, 2012: Orographic effects and evaporative cooling along a subtropical cold front: the case of the spectacular saharan dust outbreak of march 2004. *Monthly Weather Review*, **140 (8)**, 2520–2533.

Gunther, E. B., 1977: Eastern pacific tropical cyclones of 1976. *Monthly Weather Review*, **105 (4)**, 508–522.

Horel, J., and Coauthors, 2002: Mesowest: Cooperative mesonets in the western united states. *Bulletin of the American Meteorological Society*, **83 (2)**, 211–225.

Houghton, D. D., and A. Kasahara, 1968: Nonlinear shallow fluid flow over an isolated ridge. *Communications on Pure and Applied Mathematics*, **21 (1)**, 1–23.

Hsu, N., M.-J. Jeong, C. Bettenhausen, A. Sayer, R. Hansell, C. Seftor, J. Huang, and S.-C. Tsay, 2013: Enhanced deep blue aerosol retrieval algorithm: The second generation. *Journal of Geophysical Research: Atmospheres*, **118 (16)**, 9296–9315.

Huneeus, N., and Coauthors, 2011: Global dust model intercomparison in aerocom phase i. *Atmospheric Chemistry and Physics*, **11 (15)**.

IID, 2016: Salton sea air quality mitigation program. Tech. rep., Imperial Irrigation District.

IID, 2018: Salton sea hydrological modeling and results. Tech. rep., CH2M HILL.

Ives, R. L., 1949: Climate of the sonoran desert region. *Annals of the Association of American Geographers*, **39 (3)**, 143–187.

Jiang, Q., M. Liu, and J. D. Doyle, 2011: Influence of mesoscale dynamics and turbulence on fine dust transport in owens valley. *Journal of Applied Meteorology and Climatology*, **50 (1)**, 20–38.

King, J., V. Etyemezian, M. Sweeney, B. J. Buck, and G. Nikolich, 2011: Dust emission variability at the salton sea, california, usa. *Aeolian Research*, **3 (1)**, 67–79.

Lin, Y.-L., 2007: *Mesoscale dynamics*. Cambridge University Press.

Long, R. R., 1954: Some aspects of the flow of stratified fluids: Ii. experiments with a two-fluid system. *Tellus*, **6 (2)**, 97–115.

Marsham, J. H., D. J. Parker, C. M. Grams, C. M. Taylor, and J. M. Haywood, 2008: Uplift of saharan dust south of the intertropical discontinuity. *Journal of Geophysical Research: Atmospheres*, **113 (D21)**.

Mayr, G. J., and L. Armi, 2010: The influence of downstream diurnal heating on the descent of flow across the sierras. *Journal of Applied Meteorology and Climatology*, **49 (9)**, 1906–1912.

Mesinger, F., and Coauthors, 2006: North american regional reanalysis. *Bulletin of the American Meteorological Society*, **87 (3)**, 343–360.

Parajuli, S. P., and C. S. Zender, 2018: Projected changes in dust emissions and regional air quality due to the shrinking salton sea. *Aeolian Research*, **33**, 82–92.

Pokharel, A. K., M. L. Kaplan, and S. Fiedler, 2017: Subtropical dust storms and downslope wind events. *Journal of Geophysical Research: Atmospheres*, **122 (19)**.

QSA, 2003: *Quantification Settlement Agreement*. Imperial Irrigation District, and The Metropolitan Water District of Southern California, and Coachella Valley Water District, URL http://www.sdcwa.org/.

Schroeder, R. A., W. H. Orem, and Y. K. Kharaka, 2002: Chemical evolution of the salton sea, california: nutrient and selenium dynamics. *Hydrobiologia*, **473 (1)**, 23–45.

Stephen, M. F., and D. S. Gorsline, 1975: *Sedimentary aspects of the New River Delta, Salton Sea, Imperial County, California*, 276–282. Houston Geological Society.

Sweeney, M. R., E. V. McDonald, and V. Etyemezian, 2011: Quantifying dust emissions from desert landforms, eastern mojave desert, usa. *Geomorphology*, **135 (1)**, 21–34.

Todd, M., and Coauthors, 2013: Meteorological and dust aerosol conditions over the western saharan region observed at fennec supersite-2 during the intensive observation period in june 2011. *Journal of Geophysical Research: Atmospheres*, **118 (15)**, 8426–8447.

Urban, F. E., H. L. Goldstein, R. Fulton, and R. L. Reynolds, 2018: Unseen dust emission and global dust abundance: Documenting dust emission from the mojave desert (usa) by daily remote camera imagery and wind-erosion measurements. *Journal of Geophysical Research: Atmospheres*, **123 (16)**, 8735–8753.

USDI/CRA, 1974: *Salton Sea Project, California: Federal-State Feasibility Report*. 139 pp, U.S. Department of the Interior and the Resources Agency of California.

Vosper, S., 2004: Inversion effects on mountain lee waves. *Quarterly Journal of the Royal Meteorological Society*, **130 (600)**, 1723–1748.

Washington, R., and M. C. Todd, 2005: Atmospheric controls on mineral dust emission from the bodélé depression, chad: The role of the low level jet. *Geophysical Research Letters*, **32 (17)**.

Washington, R., M. C. Todd, S. Engelstaedter, S. Mbainayel, and F. Mitchell, 2006a: Dust and the low-level circulation over the bodélé depression, chad: Observations from bodex 2005. *Journal of Geophysical Research: Atmospheres*, **111 (D3)**.

Washington, R., and Coauthors, 2006b: Links between topography, wind, deflation, lakes and dust: The case of the bodélé depression, chad. *Geophysical Research Letters*, **33 (9)**.